J. Fluid Mech. (1994), *vol.* 259, *pp.* 25–45

Measurements of vortex pair interaction with a clean or contaminated free surface

By A. HIRSA† AND W. W. WILLMARTH
Department of Aerospace Engineering, University of Michigan, Ann Arbor, MI 48109, USA

(Received 11 May 1992 and in revised form 12 July 1993)

Laminar vortex pairs with small Froude number were generated by a submerged delta wing at negative angle of attack or by a pair of vertically oriented, counter-rotating flaps. The vortex pairs thus generated rise and interact with the free surface. The surface and subsurface flow field was studied using flow visualization and particle image velocimetry. Initial surface deformations, striations, are shown to be caused by stretching and interaction of cross-stream vortices near the surface. With small amounts of surface contamination, contamination fronts (producing Reynolds ridges) form on the surface and secondary vorticity, generated beneath the surface beyond the fronts, rolls up to form vortices with opposite rotation outboard of the primary vortices. The circulation associated with the secondary vortices is as much as $\frac{1}{3}$ that of the primary vortices. The secondary vortices cause the primary vortex pair to rebound from the surface. Slight surface deformations, scars, are caused by the primary and secondary vortices.

1. Introduction

Turbulence near a free surface controls many geophysical and environmental flows including mixing of pollutants in rivers as well as gas and heat exchange at an air–water interface. The interaction of turbulence with a free surface also plays a significant role in remote sensing of ships (see Munk, Scully-Power & Zachariasen 1987). The transport properties of free-surface turbulence are dominated by collisions of coherent vortical structures with the free surface, see for example Komori *et al.* (1982) and Hunt (1984). Advances in free-surface turbulence studies will undoubtedly require a fundamental understanding of the interaction of vorticity with a free surface.

An example of a vortex geometry that captures many important aspects of free-surface turbulence is the ascent and subsequent interaction of a pair of counter-rotating vortices with a free surface. Barker & Crow (1977) experimentally studied the interaction of a vortex pair with a free surface and with a solid wall. They found that the vortex pair rebounded not only from a solid wall but also from a free surface. The Froude number for the vortices was relatively low which meant that the free surface remained essentially flat. Their hypothesis for the rebounding of the vortex pair was that as a result of the interaction, the originally circular cores of the vortices were deformed into an oval shape causing them to rebound from the surface. Later, Saffman (1979) showed that the model put forth by Barker & Crow cannot explain the rebounding. Saffman showed that the observed rebounding must involve the viscosity of the fluid and cited the earlier results of Harvey & Perry (1971) who showed that

† Present address: Rensselaer Polytechnic Inst., Department of Mechanical Engineering, Aeronautical Engineering and Mechanics, Troy, NY 12180, USA.

vortex pair rebounding from a solid wall is caused by separation of the boundary layer on the wall. The mechanism for rebounding of vortices from a flat free surface remained unexplained until Bernal *et al.* (1989) experimentally showed that a vortex pair rebounds more from a highly contaminated surface than from a relatively clean one.

Recently, Ohring & Lugt (1991) performed direct Navier–Stokes calculations of the interaction of a viscous vortex pair with a clean (constant surface tension) free surface. Their calculations were for vortex pairs with relatively high Froude numbers and low Reynolds numbers. They show that a vortex pair rebounds as a result of opposite-signed vorticity produced at a deformed free surface. They also show that this type of vorticity production at a deformed free surface with no surfactant present decreases as the surface tension is increased.

The surface deformations produced during the interaction of a vortex pair with a free surface in the wake of a submerged delta wing at negative angle of attack have been studied by Sarpkaya & Henderson (1985). The initial surface deformations were striations formed normal to the wake centreline between the trailing vortices. Further downstream, as the trailing vortices approached the surface and began to spread apart they report the observation of slight surface depressions (scars) outboard of the trailing vortices and approximately parallel to the wake centreline. Following this, three-dimensional structures and dimples where vortex lines terminate at the surface were observed. Sarpkaya & Henderson compared their observations of the time and location of the above surface deformations to analytical computations of the inviscid flow field of trailing vortices approaching a wall but experimental measurements of the subsurface velocity field associated with the surface deformations have not been made.

A two-dimensional numerical calculation (Tryggvason *et al.* 1992) was made of the interaction of a vortex pair with a contaminated free surface. The Reynolds number used in the investigation was moderate and the surface was assumed to be flat (zero Froude number). The study used a simple model for the contaminants and the agreement of the numerical results with the present experimental measurements validates the model. Tryggvason *et al.* also provide a rather complete survey of the literature in theoretical work on the interaction of vortex pairs with a free surface.

In this paper we present experimental observations and measurements of the surface and subsurface flow field which occur during the interaction of a vortex pair with a free surface. To make these measurements a vortex pair generator was developed which produces a pair of laminar vortices propagating toward the surface with Froude and Reynolds numbers comparable to those measured for trailing vortices in the wake of a delta wing. The investigation is restricted to low Froude numbers so that the free-surface deformations are small and the effects of surface contamination on rebounding can be quantified.

2. Experimental apparatus and methods

The preliminary studies were carried out in the wake of a delta wing. The wing was the same size as a wing used by Sarpkaya & Henderson (1985) with a 15.2 cm chord and an aspect ratio of 1.67. The wing was mounted at a negative angle of attack of 10°. The experiments were conducted in a small towing tank with a test section that was 7.3 m long, 76 cm wide and 76 cm deep. The tank was filled with tap water and the surface was cleaned using a surface drain.

The flow field in the trailing vortices produced by the delta wing was difficult to quantify, primarily because the tow tank endwalls were far from the measurement

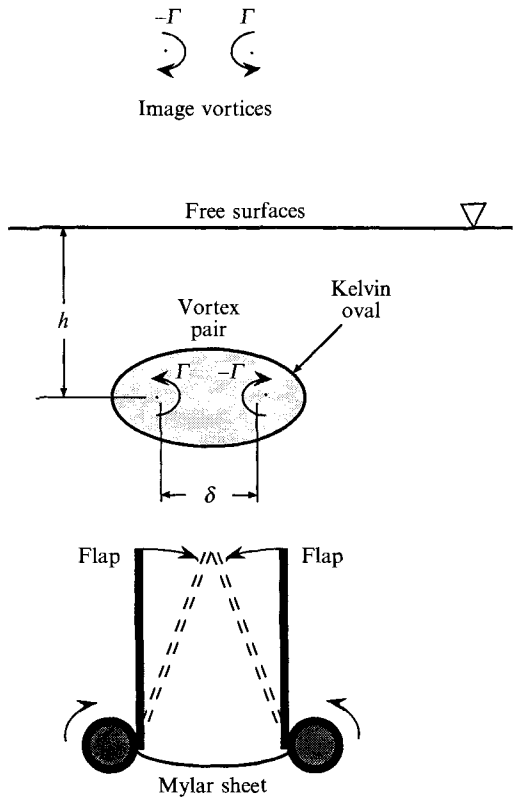

FIGURE 1. Schematic of the vortex pair generator showing vortices approaching the free surface.

plane. In order to obtain a more accessible configuration for the investigation of the flow field during the interaction of a vortex pair with the free surface a vortex pair generator consisting of a pair of counter-rotating flaps was constructed, as illustrated in figure 1. The dimensions and operating conditions of the vortex pair generator were chosen to obtain the desired Reynolds number, Re, and the Froude number, Fr. The flap separation, 12.7 cm, was equal to the span of the delta wing and the length of the flaps was 30.5 cm. The flow was found to be uniform in the central region between the endwalls. Initially the flaps were approximately vertical with the flap tips 21 cm beneath the surface and were rotated toward each other until the tips were touching to form a triangle which did not significantly obstruct the flow during creation and roll-up of the vortex pair.

The flap rotation required to produce a pair of smoothly rolled up laminar vortices which did not undergo rapid transition to turbulent flow was found by trial and error. Using the computational results of Yu & Tryggvason (1990, also personal communication), who calculated the inviscid roll-up of flat vortex sheets with various initial distributions of vorticity, as a guide the flaps were actuated with a high rate of rotation at the beginning followed by a slower motion until the flap tips were touching. This motion was programmed into a controller driving a stepping motor which actuated the flaps.

To study the effects of surfactants on the interaction of vorticity with a free surface, the free surface was cleaned and a known amount of oleyl alcohol, a surface-active agent, was placed on the surface. Oleyl alcohol is insoluble in water and a very small

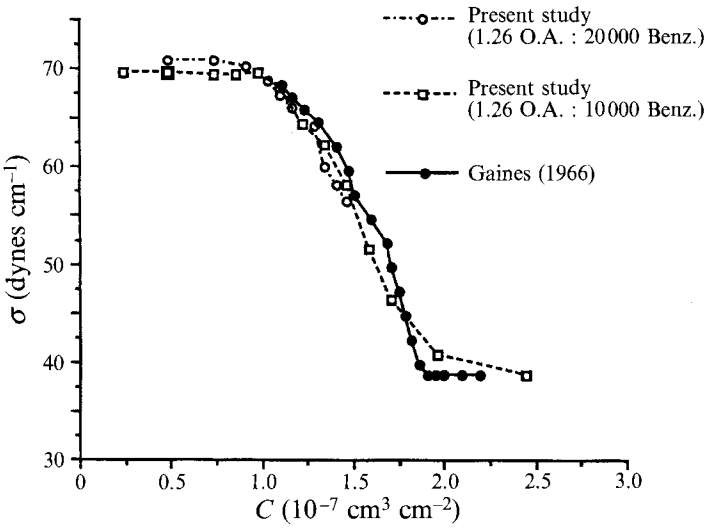

FIGURE 2. Measurement of the surface tension, σ, for various concentrations, C, of oleyl alcohol, with benzene as the dilution agent, applied to the surface of tap water.

amount on the surface forms a monomolecular film with a surface tension, σ, (dependent on concentration) less than that of pure water and ranging from approximately 37 to 72 dynes cm^{-1}. The constitutive relation for oleyl alcohol on water for two concentrations of dilute solutions is shown in figure 2. Benzene was used as the dilution agent which evaporated quickly, leaving the desired amount of oleyl alcohol on the surface (see Gaines 1966). The present measurements agree with those of Gaines, which are also plotted in figure 2. The surface tension was measured in our study using a ring-type surface tension meter (Fisher Scientific model 21 Tensiomat). With this device, as described by Du Noüy (1919), one measures the force required to pull an initially submerged platinum ring free from the water surface.

Non-invasive optical methods were used for the primary observations and measurements: the shadowgraph method for observations of the surface deformation, laser-induced fluorescence (LIF) for flow visualization and particle image velocimetry (PIV) for measurements of the velocity field. To achieve LIF flow visualization of the trailing vortices and the flap-generated vortex pairs, fluorescein was used and the flow field was illuminated using a thin sheet of blue beam (488 nm) of an argon-ion laser.

The trajectories and propagation speeds of the trailing vortices and the flap-generated vortex pairs were measured from video-taped LIF images. The apparent circulation, Γ_{app}, of the vortices was determined from the inviscid relation between the circulation, and the position and vertical component of velocity of an inviscid pair of point vortices approaching a solid wall, see Lamb (1932):

$$\Gamma_{app} = 4\pi x r^2(\partial y/\partial t)/y^2, \tag{1}$$

where x is half the distance between the vortices, y is the distance of the vortices beneath the surface and $r^2 = x^2 + y^2$.

The two-dimensional velocity field of the vortex pair during interaction with a clean or contaminated free surface was determined using the PIV technique. The velocity was determined from measurements of the distance between pairs of seed particles in doubly exposed photographs produced by pulsed illumination with a sheet of light

Vortex pair	δ_0 (cm)	Γ_{app} (cm^2 s^{-1})	*Re*	*Fr*
1	6.40	110	11000	0.22
2	7.73	156	15600	0.23

TABLE 1. Parameters of the vortex pairs generated with the vortex pair generator with $\nu = 0.01$ cm^2 s^{-1}

from a copper vapour laser. The doubly exposed images of the tracer particles were analysed by illuminating (interrogating) a small spot on the negative with a helium-neon laser. The scattered light from pairs of particles within the illuminated spot was collected and imaged by a lens system to produce a Young's fringe pattern which was recorded and processed, using a video system and an image analyser, to determine the fringe spacing and orientation. The fring spacing is inversely proportional to the flow speed and the fringes are oriented normal to the flow direction. Since the flow was laminar, the 180° uncertainty in the flow direction was easily resolved. Kwon (1989) presents additional information about the image analysis system. For further information on the experimental apparatus and methods see Hirsa (1990).

3. Investigations in the wake of a delta wing

Our initial investigation was a visual survey of the free-surface deformations as well as LIF images of the subsurface flow in the wake of a delta wing. The Reynolds numbers of the trailing vortices, defined by $Re \equiv \Gamma/\nu$ (where Γ is the circulation and ν is the kinematic viscosity), were in the range 9200 to 20200 and the corresponding Froude numbers, as defined by $Fr \equiv \Gamma/(g\delta_0^3)^{\frac{1}{2}}$ (where g is the gravitational acceleration and δ_0 is the spacing of the vortices before the interaction with the surface) were in the range 0.096 to 0.21. At these low Froude numbers surface deformations are small during the interaction of the vortices with the free surface.

As described by Sarpkaya & Henderson (1985), who studied relatively stronger trailing vortices, with $22000 \leqslant Re \leqslant 66000$ and $0.34 \leqslant Fr \leqslant 1.1$, the first surface deformations, the striations, appeared when the rising vortex pair had reached a distance beneath the surface comparable to the spacing between the vortices. During the next stage of the interaction process, instead of the scars observed by Sarpkaya & Henderson we observed very sharp surface deformations, Reynolds ridges (described below), which appeared on each side and approximately above the centre of each trailing vortex.

After the Reynolds ridges first became visible they moved outward as the distance between the trailing vortices increased owing to the interaction of the subsurface vortices with their images above the surface. This outward movement was accompanied by an increase in length of the striations and was soon followed by the appearance of numerous elongated surface depressions and dimples outboard of the trailing vortices. At approximately this time the intensity of the striations began to decrease.

Video-taped recordings of different realizations were made which showed that the motion of particles on the surface was not always repeatable and the particle motion was found to depend upon the type of particles used as passive markers. This implied that the condition of the free surface had a fundamental effect on the interaction of the trailing vortices with the free surface. The problem with surface contamination is that surface-active agents tend to accumulate on the free surface of any water sample, even when the sample is covered. Scott (1975) describes methods to prepare clean water for

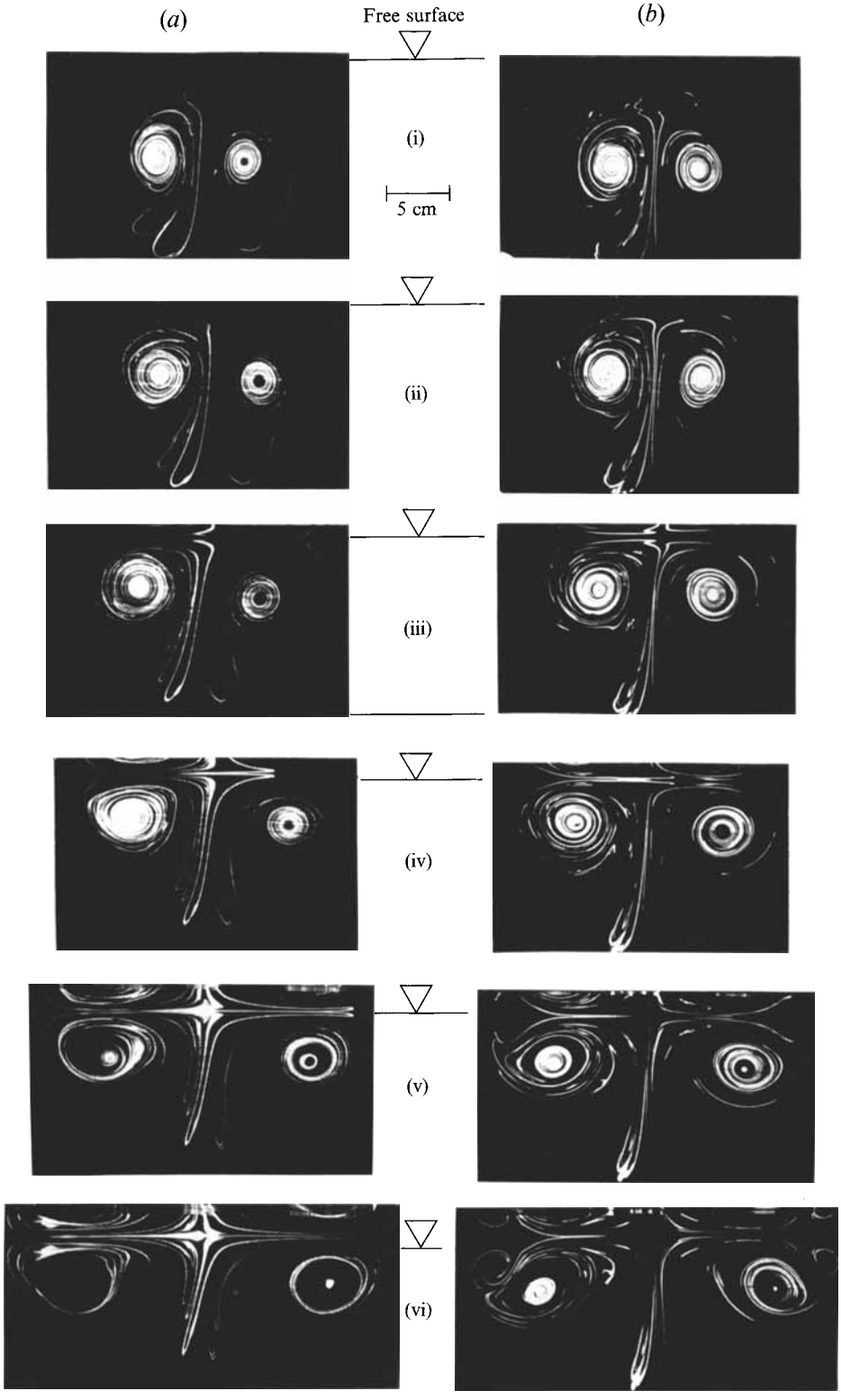

FIGURE 3. LIF photograph of vortex pair 1 interacting with a free surface: (a) no surfactant added, (b) with oleyl alcohol added with $\pi = 2.5$ dynes cm^{-1}. (i) $\tau^* = -0.11$, (ii) $\tau^* = 0.30$, (iii) $\tau^* = 0.70$,

fluid mechanical experiments with an uncontaminated surface. In another paper, Scott (1982) describes measurements of the formation of a Reynolds ridge on the surface at the edge of a stagnant surface film. The ridge is produced at the leading edge of a boundary layer formed beneath a contaminated surface when a uniform flow of fluid with contaminants on the surface is blocked by a barrier which penetrates below the surface. The boundary layer formed upstream of the barrier is a result of a balance between shear forces in the viscous flow beneath the surface and the surface shear force produced by gradients in surface tension. These gradients in surface tension result from concentration gradients in the blocked film of surface contaminants. At the leading edge of the contaminated surface the clean upstream fluid near the surface is rapidly decelerated with a correspondingly rapid increase in surface elevation. This phenomena is observable to the eye or with the aid of a shadowgraph system as a narrow ridge.

4. Flow visualization and measurements in a cross-sectional plane of vortex pairs

Two laminar vortex pairs (1 and 2) with similar Froude number but rather different Reynolds numbers were selected for study during this investigation. The choice of the vortex pairs was based on the fact that vortices were strong enough to redistribute the initially uniform surfactant on the free surface and yet remained laminar during the interaction process. The distance between the apparent centres of these vortices and the average distance of the apparent centres beneath the surface was plotted as a function of time, and the apparent circulation was determined from (1). Table 1 lists the properties of the two vortex pairs used in this investigation.

In order for comparisons to be made of the interaction with the free surface of vortex pairs generated at various depths and of different strengths and sizes, a dimensionless time, τ^*, was defined as

$$\tau^* = \frac{t - t_1}{\delta_0 / v_{p0}}. \tag{2}$$

Here, t is the time since the start of the flap motion, t_1 is the time elapsed from the start of the flap motion until the time the vortices are at a depth equal to δ_0, and v_{p0} is the propagation speed before the interaction with the free surface.

When a vortex pair arrives at the free surface, the fluid carried within the Kelvin oval is deposited on the surface and this may change the condition of the free surface above the vortex pair. The boundary of the fluid transported by vortex pair 1 was visualized using LIF when fluorescein dye was injected in the fluid between, adjacent to and above the flaps. After the vortex pair was fully rolled up, prior to interaction with the free surface, the boundary of the fluid transported by the vortices showed unsymmetrical entrainment and detrainment patterns above and below the transported fluid. The width and the height of the transported fluid volume were approximately equal to twice the spacing between the apparent centres of the vortex pair.

4.1. *Vortex pair interaction with a clean free surface*

All the experiments were performed using tap water because it was not economically feasible to provide the large quantity of distilled water required for the vortex pair experiments. After filling the tow tank with tap water the surface above the vortex pair

(iv) $\tau^* = 1.10$, (v) $\tau^* = 1.50$, (vi) $\tau^* = 1.90$ (approximate scale: the distance between vortex centres in (i) = 7.7 cm).

generator was cleaned, as described earlier. The surface tension was then measured. It was found that, owing to the residual surface contamination, the surface tension was slightly less (of the order of 1.0 dyne cm^{-1} less) than the surface tension of pure water at the same temperature. Experiments, described below, with this cleaned surface showed that the residual surface contamination caused the formation of a Reynolds ridge well outboard of each vortex with no measurable effect on the trajectories of the vortices during their interaction with the surface.

The flow field for vortex pair 1 generated beneath a clean free surface at Reynolds number 11000 (see table 1) was visualized using LIF and representative photographs of the cross-sectional plane are shown on the left side (*a*) of figure 3. The photographs, figure 3 (i)–(vi), show the vortex pair at equal τ^* intervals of 0.4 beginning with $\tau^* = -0.11$. The mirror image that appears on the upper portion of many of the photographs is due to total internal reflection at the free surface.

The average trajectory of the right-hand vortex beneath a clean surface is indicated by the long-dashed line in figure 4. Hirsa (1990) presents a plot comparing the trajectories of vortex pairs 1 and 2, beneath the cleaned free surface, with the trajectory of an inviscid vortex pair approaching a wall that shows that both trajectories deviate by less than 10% from the inviscid trajectory. It should be noted that in figure 3(*a*) and in figure 4 there is no observable rebounding of the vortex pair from the clean surface.

4.2. *Vortex pair interaction with a contaminated surface*

The flow field for vortex pair 1 generated beneath a contaminated free surface was visualized and is shown on the right side (*b*) of figure 3. The surface was initially covered with oleyl alcohol with a surface pressure, $\pi = 2.5$ dynes cm^{-1}. Here, and in the remainder of the paper, the degree of surface contamination by oleyl alcohol is specified by the surface pressure, π, which is the surface tension of the cleanest water minus the surface tension with oleyl alcohol placed on the surface. The vortex pair beneath the contaminated surface is rebounding from the surface and in figure 3(*b*, vi) is further below the surface than at the earlier time, see figure 3(*b*, iv), when the distance between the vortex pair and the surface was a minimum. As will be shown below in the discussion of the PIV measurements of the velocity field, the presence of the surface-active agent has led to the generation of secondary vorticity beneath the free surface. In figure 3(*b*, vi), the secondary vorticity outboard of the primary vortices, has rolled up to form vortices with sign opposite to the nearby primary vortices. As a result of the mutual induction between the primary and adjacent secondary vortices, the primary vortices are moving downward and outward in figure 3(*b*, vi).

The averaged trajectories of the right-hand primary and secondary vortices beneath a free surface with different amounts of surface contamination and beneath a solid wall are shown in figure 4. During the interaction with a contaminated surface, the primary vortex pair rebounded from the surface at a distance of the order of $\frac{1}{2}\delta_0$ beneath the surface. The amount of rebound increased when the surface concentration of oleyl alcohol was increased. The times that the rolled-up secondary vortices were first observed are listed in the caption of figure 4. Also, tic marks on the trajectories of the primary vortices indicate their position when the rolled-up secondary vortices were first observed. Note that the location of the tic marks on the primary vortex trajectories show that the primary vortices were already rebounding from the surface owing to the velocity induced by the secondary vorticity before the secondary vortices were fully formed. Note also that the trajectory of the primary vortices beneath a solid wall and beneath a severely contaminated free surface, $\pi = 18$ dynes cm^{-1}, were approximately the same. In both cases secondary vortices were present but, unlike beneath a solid

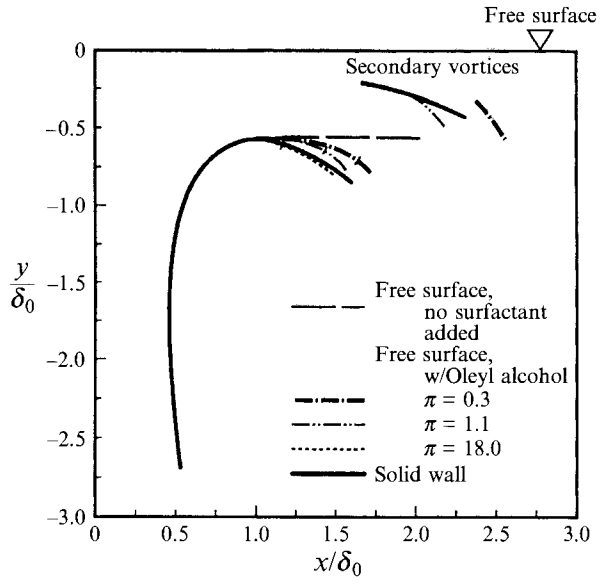

FIGURE 4. Average trajectory of the apparent centre of the right-hand primary and secondary vortices during the interaction of vortex pair 1 with various surface conditions. The primary vortex location when the apparent centre of the secondary vortex was observable is indicated by a tick mark. The duration of the primary and secondary trajectories are: free surface, ($\pi \approx 0$) $-1.83 \leqslant \tau^* \leqslant 2.58$, not formed; free surface ($\pi = 0.3$) $-1.83 \leqslant \tau^* \leqslant 2.58$, $2.18 \leqslant \tau^* \leqslant 2.58$; free surface ($\pi = 1.1$) $-1.83 \leqslant \tau^* \leqslant 2.18$, $1.78 \leqslant \tau^* \leqslant 2.18$; free surface ($\pi = 18$) $-1.83 \leqslant \tau^* \leqslant 1.78$, turbulent; solid wall $-1.83 \leqslant \tau^* \leqslant 2.18$, $1.38 \leqslant \tau^* \leqslant 2.18$.

wall, the secondary vortices beneath the highly contaminated free surface were turbulent and are not shown because repeatable trajectory data could not be determined.

The present results are in qualitative agreement with earlier findings by Bernal *et al.* (1989), which showed that a strong vortex pair ($Re = 1800$ and $Fr = 1.45$) rebounds more from a highly contaminated surface than a clean surface. It should be noted that the rebounding observed by Bernal *et al.* was partially due to the large Froude number of the vortex pair causing the surface to deform significantly.

4.3. *PIV measurements of vortex pairs near the free surface*

The velocity field measured with the PIV technique during the interaction of vortex pair 1 with a clean free surface at the time $\tau^* = 0.58$ is shown in figure 5. The apparent centres of the vortices were approximately 5 cm beneath the free surface and 12 cm apart. The dynamic range of the set-up did not allow measurements near the vortex cores and the stagnation point. One of the most significant properties of the flow field is the nearly uniform outward surface and subsurface velocity above and outboard of the primary vortices. This is in marked contrast, as described below, to the magnitude and direction of the velocity components above and outboard of the primary vortices when the surface is contaminated.

PIV measurements of the velocity field before interaction with the surface were also made for vortex pair 1 and the circulation about the vortices was calculated by integrating $\boldsymbol{u} \cdot \mathrm{d}\boldsymbol{l}$ around a rectangular contour enclosing a vortex (see Hirsa 1990). The magnitude of circulation was found to be 146 $\mathrm{cm}^2\ \mathrm{s}^{-1}$. The apparent circulation, based on a point-vortex model, was found to be 110 $\mathrm{cm}^{-2}\ \mathrm{s}^{-1}$.

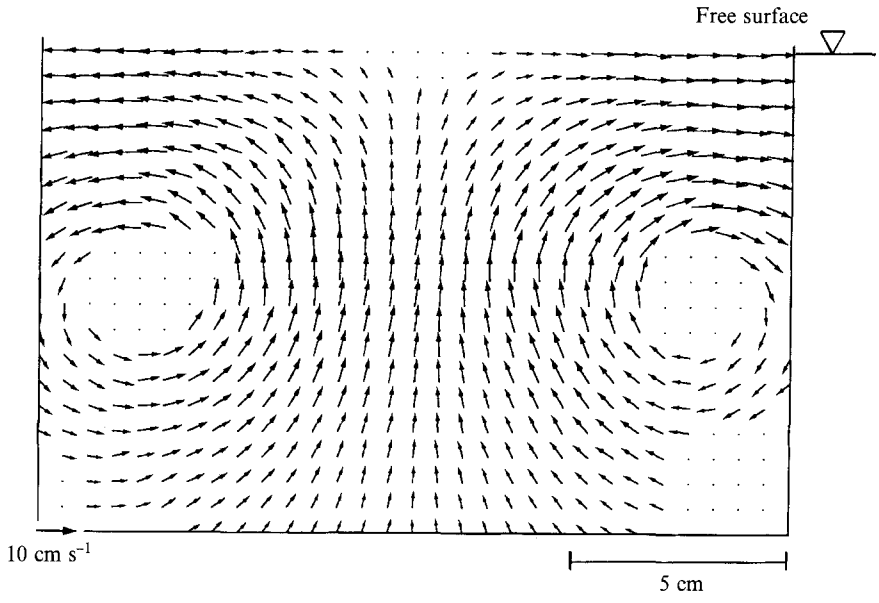

FIGURE 5. Vortex pair 1 velocity field during interaction with a free surface at time $\tau^* = 0.58$. No surfactant added.

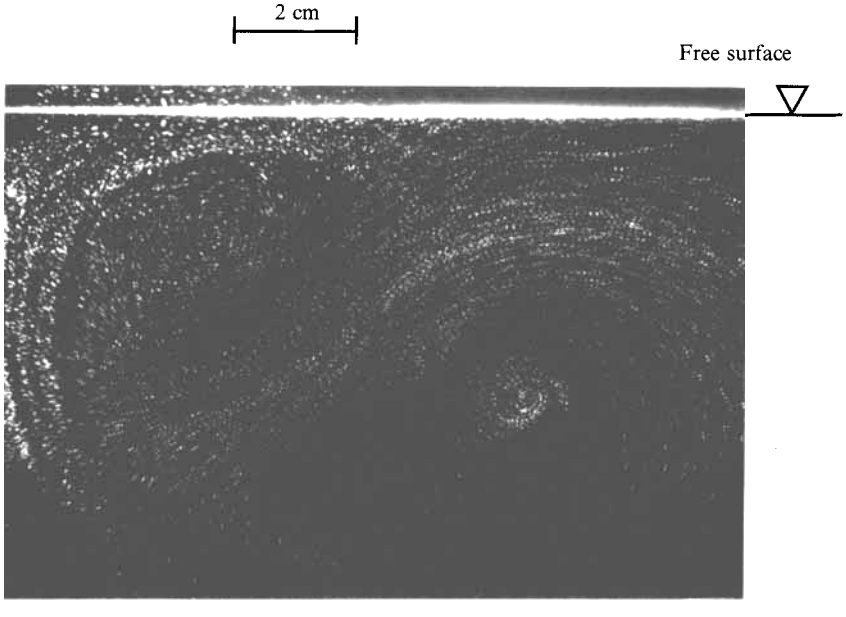

FIGURE 6. Doubly exposed particle image photograph of the left-hand primary and secondary vortices during the interaction of vortex pair 1 with a free surface covered with oleyl alcohol ($\pi = 18.0$ dynes cm^{-1}), at time $\tau^* = 1.82$. The primary vortex is 10 cm away from the centreline.

As an example, a typical doubly exposed photograph of particles in the flow within and outboard of the left primary vortex during interaction of vortex pair 1 with a contaminated free surface is shown in figure 6. The velocity vector plot associated with this photograph is shown in figure 7 and was obtained at the time $\tau^* = 1.82$ when the

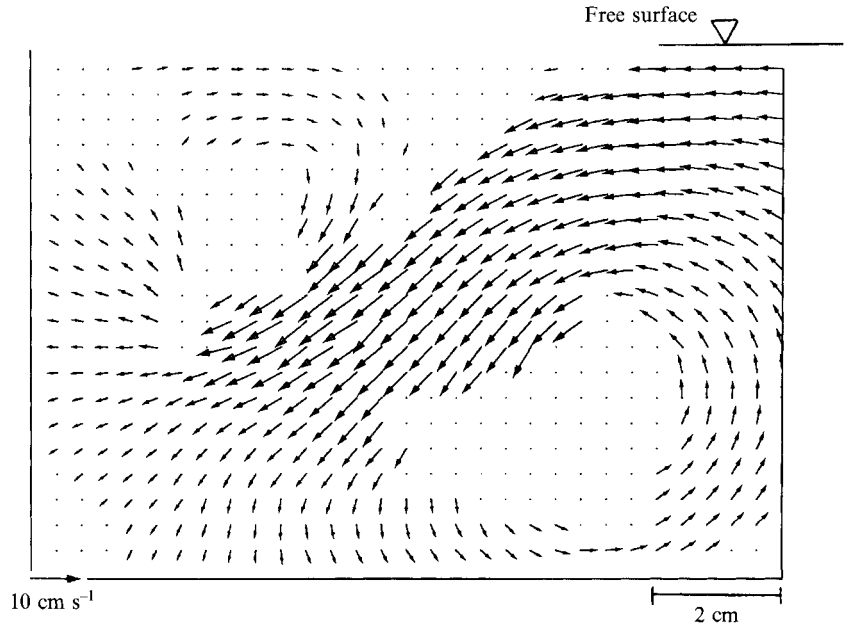

FIGURE 7. Velocity field determined from the negative image of the photograph of figure 6 showing the primary and secondary vortices produced during interaction of vortex pair 1 with a contaminated surface, $\pi = 18.0$ dynes cm^{-1}, at time $\tau^* = 1.82$. The right edge of the figure is 7.7 cm from the centreline.

vortex pair was rebounding from the contaminated surface. At this time the vortex pair position relative to the surface is approximately the same as for the vortex pair shown in figure 3(*b*, vi) although the free surface was more contaminated ($\pi = 18$ dynes cm^{-1} for figures 6 and 7 as compared to $\pi = 2.5$ dynes cm^{-1} in figure 3*b*). A rolled-up vortex outboard of the primary vortex, formed from secondary vorticity generated beneath the contaminated free surface, can be clearly observed in figure 7. The downward and outward velocity induced by the secondary vortex on the primary vortex is clearly the cause of the observed rebounding of the primary vortices when the free surface is contaminated. The circulation associated with the secondary vortex shown in figure 7 was calculated around a square 10 divisions on a side, approximately centred on the secondary vortex. The circulation was approximately -45 (cm^2 s^{-1}), which is about one third of the magnitude of the primary vortex. This indicates that the quantity of secondary vorticity generated during the interaction of the primary vortices with a highly contaminated surface is indeed significant.

5. The effect of surface contamination on surface deformations

5.1. *Clean surface*

Figure 8 contains four shadowgraph views of the right half of the clean free surface when vortex pair 2 was a distance less than δ_0 beneath the surface. In figure 8(*a*), a number of striations normal to the centreline of the vortex pair have already formed and are visible. In addition to the striations, a Reynolds ridge, the thin slightly undulating line approximately parallel to the centreline, is visible outboard of the ends of the striations.

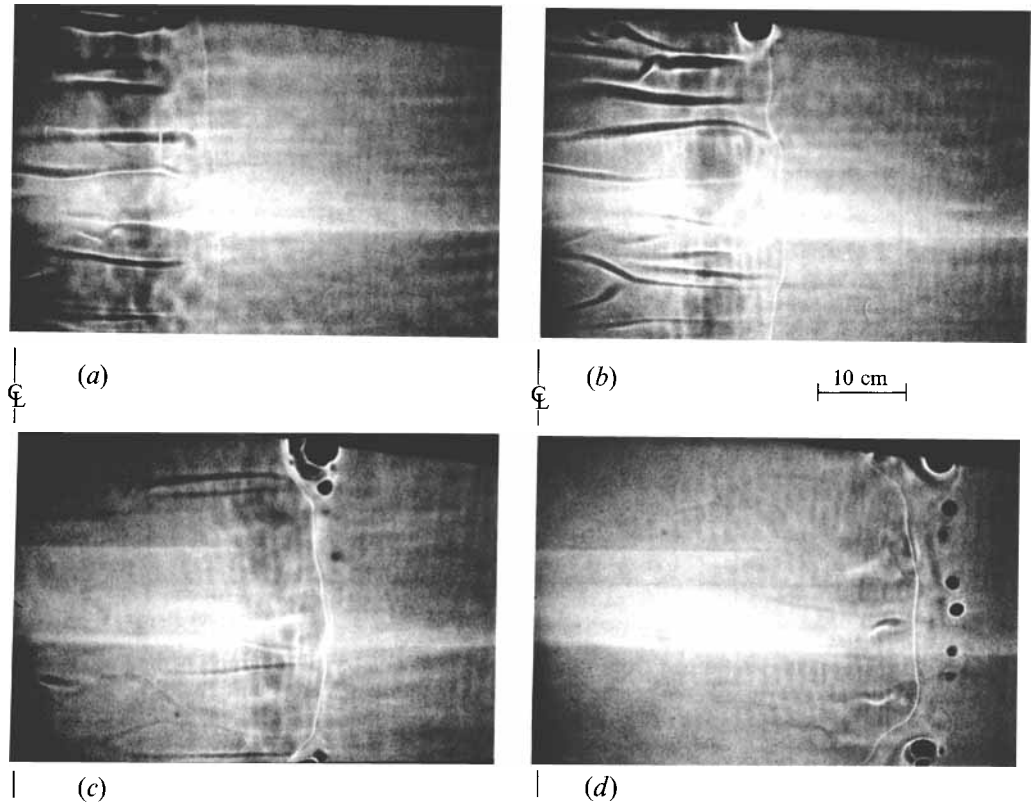

FIGURE 8. Shadowgraph views of the right half of the free surface during the interaction of vortex pair 2 with a free surface with no surfactant added. The times are: (*a*) $\tau^* = 0.93$; (*b*) $\tau^* = 1.37$; (*c*) $\tau^* = 2.24$; (*d*) $\tau^* = 3.10$. Note that the centreline is near the left edge of each photograph.

A Reynolds ridge would not be formed if the surface were absolutely clean and free of contaminants. However, as described earlier, tap water contained dissolved contaminants which could not be completely removed. During the approach of the vortex pair to the free surface the relatively clean water carried with the vortex pair has reached the surface and pushed the existing surface contaminant outward until a contamination front was formed. It should be emphasized that the water between the centreline and the Reynolds ridge is moving outward as shown in the PIV vector plot of figure 5. The trajectory data measured for this vortex pair (pair 2) and for vortex pair 1, shown in figure 4, indicate that the small amount of contamination remaining on the surface after cleaning, which was swept outboard of the primary vortices to form the Reynolds ridge, did not affect the trajectory of the vortex pairs.

Also faintly visible in figure 8(*a*) is a rather wide dark region, a depression, parallel to the centreline inboard of the ends of the striations and to the left of the Reynolds ridge. This surface depression or scar is located above the core of the primary vortex. The depression is caused by the higher speed outward flow between the primary vortex and its image.

In the subsequent photographs, figure 8(*b–d*), the Reynolds ridge remains outboard of the scar above the vortex core as both move outward to the right. In figure 8(*c*, *d*), the striations near the centreline appear to have become weaker and in figure 8(*d*) the ends of the striations are still visible to the left of the Reynolds ridge while circular dark regions, dimples, have formed outboard of the Reynolds ridge. The dimples appeared

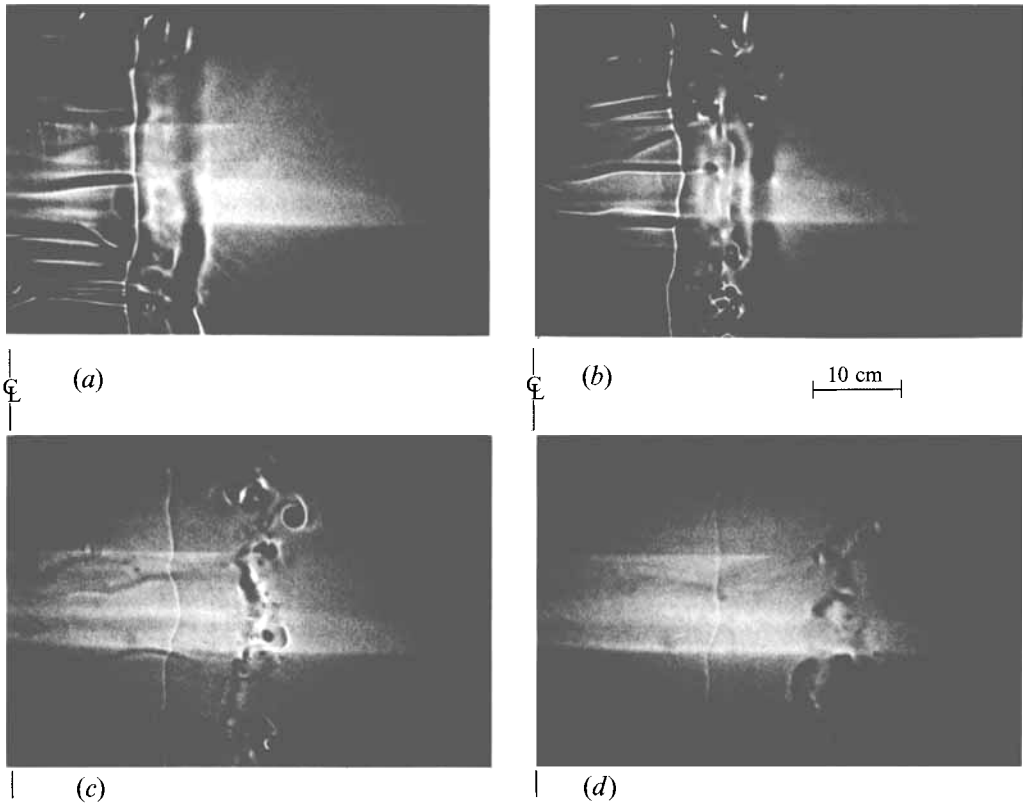

FIGURE 9. Shadowgraph view of the right half of the free surface during the interaction of vortex pair 2 with a free surface with oleyl alcohol added, $\pi = 0.3$ dynes/cm. The times are: (*a*) $\tau^* = 0.93$; (*b*) $\tau^* = 1.37$; (*c*) $\tau^* = 2.24$; (*d*) $\tau^* = 3.10$.

to be the ends of the striations, since the number of dimples was always of the same order as the number of striations that were visible earlier. A large dimple has appeared at the top of figure 8(*c*) and it and another at the bottom are visible in figure 8(*d*). These are believed to be the result of the formation of endwall vortices (see Yamada & Honda 1989).

5.2. *Slightly contaminated surface*

Figure 9 is a sequence of four shadowgraph views of the surface deformations observed during the interaction of vortex pair 2 with the surface contaminated with a small amount of oleyl alcohol with surface pressure $\pi = 0.3$ dynes cm^{-1}. The striations and the Reynolds ridge are again visible in the first figure 9(*a*) but the distance from the centreline to the Reynolds ridge is less than in figure 8(*a*) and the striations are not as long as they were at the same dimensionless time for the clean surface. In addition, two scars parallel to the centreline are visible in figure 9(*a*), one above the core of the primary vortex which is directly below the Reynolds ridge and another more distinct scar, to the right of the Reynolds ridge, which is caused by the secondary vorticity generated beneath the contaminants on the free surface outboard of the Reynolds ridge.

As the interaction continues, in figure 9(*b*) the two scars and the Reynolds ridge have moved outwards. The striations now extend outboard of the Reynolds ridge and small surface depressions have begun to form near the ends of the striations. In the last two

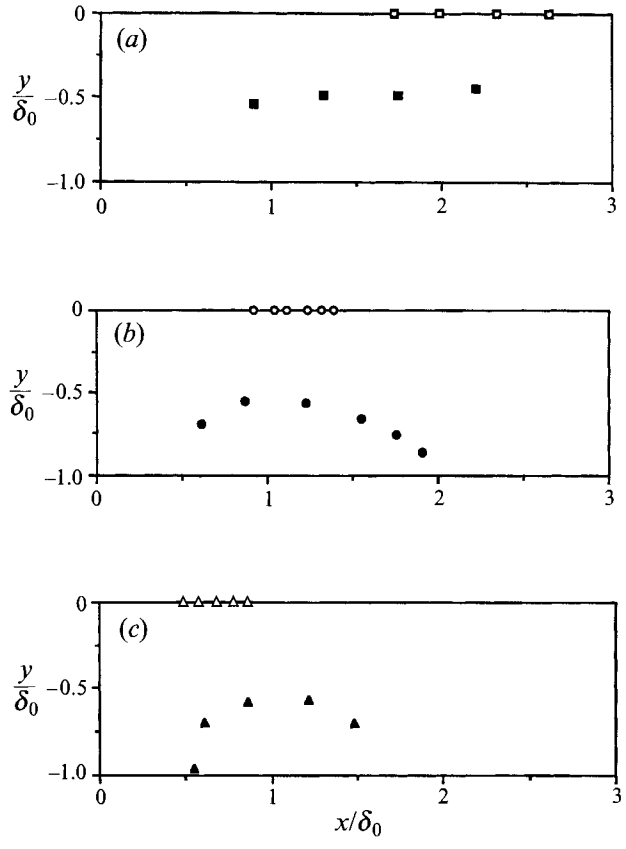

FIGURE 10. The position of the apparent centre of the right-hand vortex (solid symbols) and Reynolds ridge (open symbols) during interaction of vortex pair 2 with the free surface at equal increments of time, $\Delta\tau^* = 0.38$. The distance from the centreline, x/δ_0, increases monotonically for all the data points shown. (*a*) No surfactant added to the surface for time interval, $0.82 \leqslant \tau^* \leqslant 1.97$. (*b*) Oleyl alcohol added to the surface, $\pi = 0.3$, for time interval, $0.45 \leqslant \tau^* \leqslant 2.36$. (*c*) Oleyl alcohol added to the surface, $\pi = 1.1$, for time interval $0.06 \leqslant \tau^* \leqslant 1.59$.

views, the scars above the primary and secondary vortices and the striations all have moved somewhat further outwards and have begun to fade away leaving the outward-moving dimples and random surface depressions.

The above observations suggest that the location of the Reynolds ridge relative to the location of the primary vortex depends upon the strength of the primary vortices and the degree of surface contamination. Figure 10 is a plot of the position of the primary vortices and Reynolds ridge non-dimensionalized by δ_0 at discrete values of non-dimensional time, τ^*, for vortex pair 2. From this plot it can be observed that the Reynolds ridge was formed closer to the centreline and at an earlier time when the surface contamination was increased. It can also be observed that the convection speed of the Reynolds ridge is reduced as the surface contamination increases.

5.3. *Highly contaminated surface*

Figure 11 is a shadowgraph view of the surface during the interaction of vortex pair 2 with the surface contaminated with a relatively large amount of oleyl alcohol with $\pi = 31$ dynes cm^{-1}. The dimensionless time in this case is $\tau^* = 0.82$, approximately the same as for figure 9(*a*), but unlike the vortex pair interaction with a less contaminated

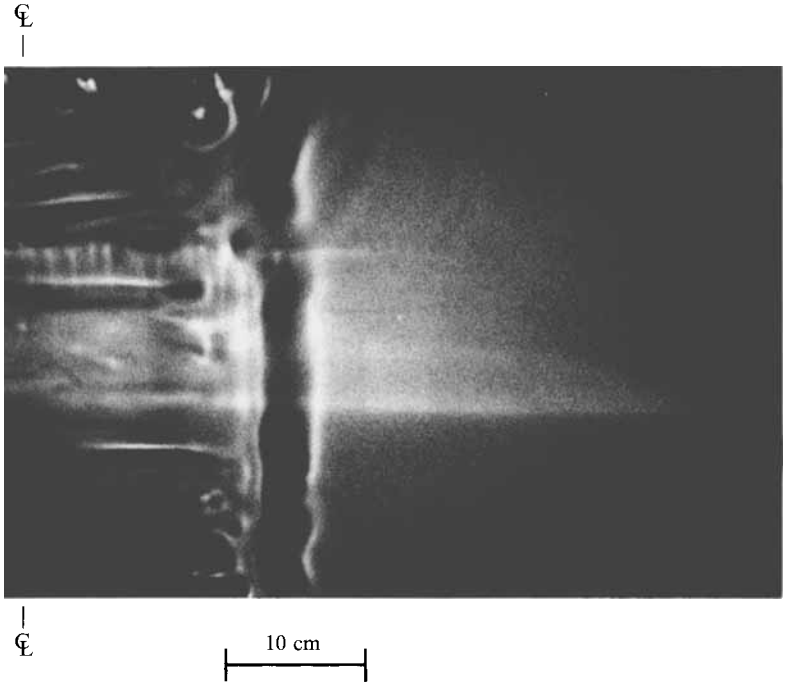

FIGURE 11. Shadowgraph view of the free surface showing an intense scar produced during the interaction of vortex pair 2 with the free surface when a high concentration of oleyl alcohol was present on the surface, $\pi = 31$ dynes cm^{-1}. The time is $\tau^* = 0.82$.

surface shown in figure 9(*a*), the surface film has not been ruptured by the upwelling of fluid contained in the Kelvin oval and consequently a Reynolds ridge has not formed. The striations are visible as well as an intense scar above the centre of the secondary vortex and a much less intense scar above the primary vortex inboard of the ends of the striations. The difference between the intensity of the scars is dependent on the distance of the vortices from the surface and their strength.

The observation of scars, elongated surface depressions in a direction approximately parallel to the centreline of the wake and outboard of the centre of the primary vortices, were reported by Sarpkaya & Henderson (1985). In the present experiments, for weaker vortices, shadowgraph observations showed scars directly above the centre of the primary vortex cores and, when rolled-up secondary vortices were formed beneath contaminated surfaces, scars were observed directly above the centres of the secondary vortices as well. For highly contaminated surfaces, the primary vortices rebounded from the surface leaving the rolled-up secondary vortices close to the surface (see figure 3*b*) and the scar above the centre of the secondary vortex core was outboard of the centre of the primary vortex core and much more intense, as illustrated in figure 11. No scar-type surface depressions outboard of the primary vortices were observed when the free surface was clean.

6. Investigation of the flow field associated with the striations

The striations (Sarpkaya & Henderson 1985) were always the first surface deformations to be observed, but no measurements of the surface deformations or the velocity field accompanying the striations have been reported. The fact that the striations first appear as irregular slightly elongated disturbances on the surface

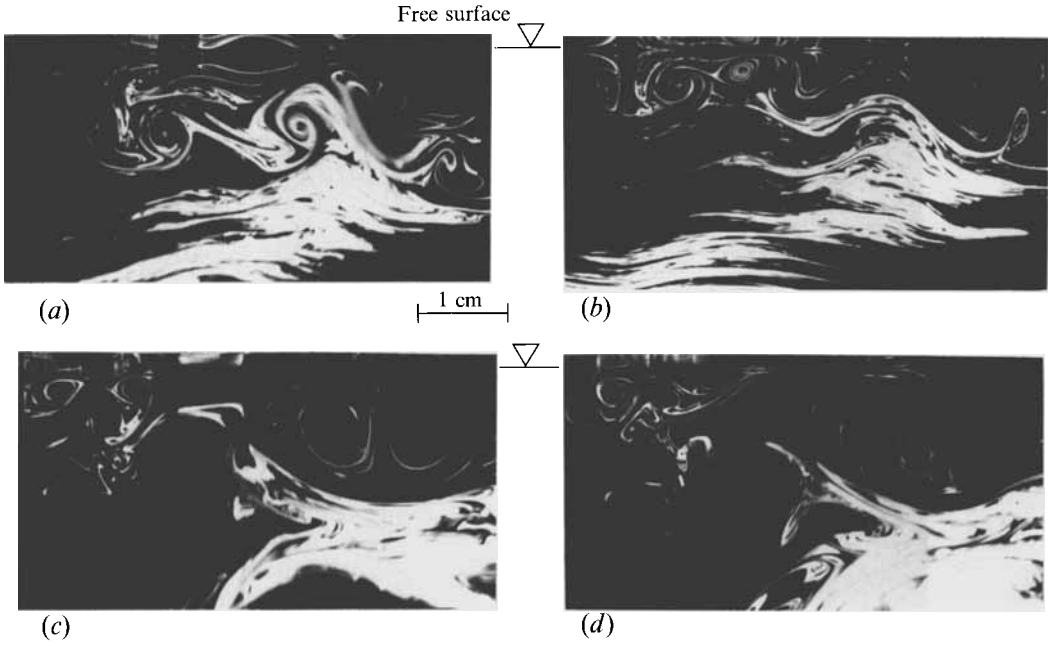

FIGURE 12. Successive cross-sectional views (10 cm or $1.3\delta_0$ from the centreline) of the LIF images of cross-stream vortices associated with the striations during the interaction of vortex pair 2 with a clean free surface. The time for each photograph is: (*a*) $\tau^* = 0.84$, (*b*) $\tau^* = 0.96$, (*c*) $\tau^* = 1.30$, (*d*) $\tau^* = 1.41$.

between the trailing vortices (or vortex pairs produced with the flaps) and then become highly elongated in a direction normal to the cores of the vortices suggests that the striations are caused by the stretching of random vorticity in the upwelling flow field of the primary vortices as they approach the surface.

These observations provided the motivation which led to the construction of a flow visualization set-up in the wake of the delta wing allowing simultaneous shadowgraph observations of the surface deformations and LIF observations of the flow field in a plane parallel to the cores of the trailing vortices and normal to the surface. Experiments conducted with this set-up showed that a cross-stream vortex was always observed beneath each striation.

In figure 12, photographs are shown of the subsurface flow field of the cross-stream vortices observed in a plane normal to the surface and parallel to the vortex pair cores 10 cm ($1.3\delta_0$) from the centreline of the vortex pair generator for a single realization of vortex pair 2 interacting with a clean free surface. The first photograph, figure 12(*a*), was taken when the primary vortex was not yet at the plane of the light sheet and several distinct cross-stream vortices are visible in this photograph. The second photograph, figure 12(*b*), was taken slightly later when the primary vortex had entered the plane of the light sheet. The cross-stream vortices near the surface appear quite energetic. The last two photographs, figure 12(*c*, *d*), show the evolution of the cross-stream vortices near the free surface.

During the course of the experiments with the delta wing and the vortex pair generator, the tendency for the formation of pairs of striations (pairing) was often observed, see for example figure 8(*a*, *b*). Figure 13 shows an exceptional shadowgraph view of the interaction of vortex pair 2 with a clean free surface in which eight striations that were visible on the surface were all in the process of pairing. The primary vortex in figure 13 appears as a slightly darkened region on the surface inboard of the ends

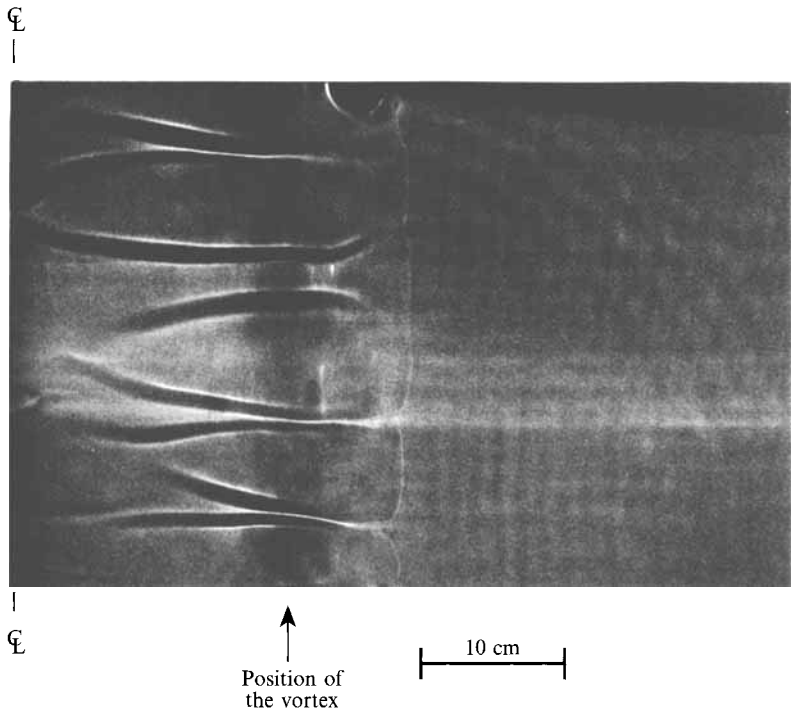

FIGURE 13. Shadowgraph view of the clean free surface during the interaction of vortex pair 2 with the surface. The simultaneous pairing of eight striations is visible.

of the paired striations. The fact that the striations are caused by cross-stream vortices near the surface suggests that the pairing of the striations is caused by mutual induction between the cross-stream vortices and their images above the free surface.

The pairing observed in the photograph in figure 13 occurs predominantly between the centreline and the location of the primary vortex core. This behaviour appears to be caused by the increased rate of strain, along the axes of the cross-stream vortices, and the upward convection velocity in the flow field of the primary vortices. Numerical calculations of an inviscid pair of point vortices approaching a wall for values of y near the surface, $-\frac{1}{4}\delta_0 \leqslant y \leqslant 0$, show that the regions of maximum upward velocity occur at approximately the same location as the maximum value of $\partial u/\partial x$, which moves outward with the primary vortex. This suggests that the rapid pairing and intensification of the striations inboard of the primary vortices, as observed in figure 13, is caused by the increased stretching and the upward convection of the cross-stream vortices in this region near and inboard of the primary vortex. This increased stretching would result in higher velocities in the vortex cores and the increased upward convection would bring the cross-stream vortices nearer to the surface, resulting in greater surface depressions appearing as more intense striations.

The spatial uniformity of the pairing of the cross-stream vortices visible in figure 13 is unusual. This uniformity suggests that the cross-stream vortices observed in figure 13 are formed by the stretching of a single vortex imbedded in the fluid carried to the surface by the vortex pair. Perturbations along this vortex cause it to be stretched back and forth between the primary vortices, and mutual induction of this stretched vortex and its image leads to the uniform formation of paired cross-stream vortices from individual vortices with equal and opposite circulation. A similar situation was modelled by the calculations of Tryggvason *et al.* (1991) in which a weak, sinusoidally

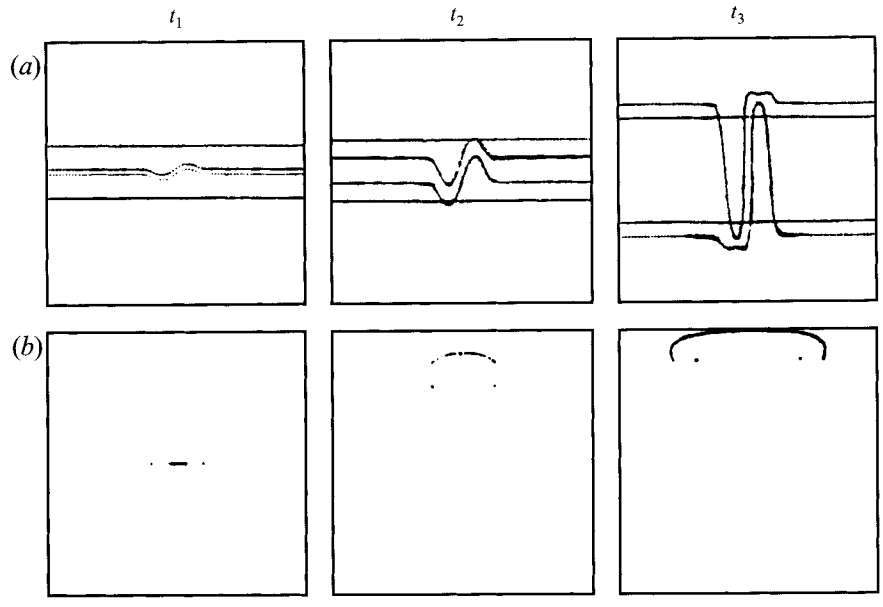

FIGURE 14. Deformation of a weak vortex pair placed between a stronger pair at three different times; (*a*) top view, (*b*) side view. Reprinted from Tryggvason *et al.* (1991) by permission of the American Mathematical Society.

perturbed vortex pair is placed in the centre of a stronger vortex pair approaching the surface, as shown in figure 14. The weak pair is observed to stretch across the larger vortex pair, producing cross-stream vortices.

The apparent circulation about the cross-stream vortices was calculated from the propagation speed of isolated cross-stream vortices parallel to the surface and the distance of their centres beneath the surface produced by vortex pair 2. The results showed that the magnitude of the circulation about the cross-stream vortices was of the order of $\frac{1}{15}$th of the apparent circulation about the primary vortices.

The distribution and intensity of the striations in the wake of the delta wing appeared to be more random than similar quantities on the surface above vortex pairs 1 or 2 when the Reynolds numbers were of the same order. At high towing speeds of the delta wing the initial random surface distributions (which become striations) were observed to be more numerous and intense than at low towing speeds. In an attempt to quantify one aspect of the striations, the average distance, $\bar{L}$, between the striations was measured for different towing speeds with the delta wing at a depth of 10 cm. The average spacing and the standard deviation as a function of Reynolds number of the trailing vortices are plotted in figure 15 and show that $\bar{L}/\delta_0$ is in the range of 0.15–0.22. The decrease in the average spacing between the striations as the Reynolds number increases appears to be significant.

Sarpkaya & Suthon (1991) studied vortex pairs in the laboratory by pumping fluid through a converging two-dimensional nozzle and measured the spacing between the striations, $\bar{L}/\delta_0$, to be between 0.38 and 0.63 which is different from the present results for the striations produced by the delta-wing trailing vortices. Sarpkaya & Suthon suggested that the striations are a result of Crow short-wave instability producing waviness on the outside of the rising Kelvin oval as it interacts with the free surface.

Recently, Locke, Hirsa & Rubin (1993) (also see Locke 1993) have conducted experiments using a flap-type vortex pair generator similar to the present apparatus

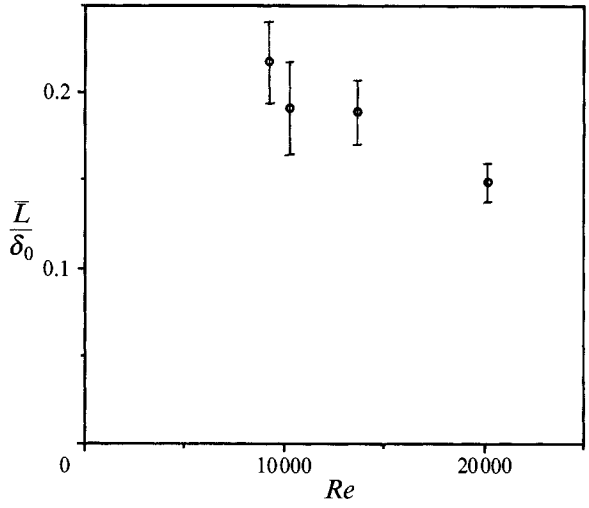

FIGURE 15. Average dimensionless distance between the striations, $\bar{L}/\delta_0$, as a function of Reynolds number (based on apparent circulation) for trailing vortices in the wake of the delta wing.

that show spatially periodic pairs of cross-stream vortices forming around each core of the vortex pair as the vortex pair propagates horizontally without any interaction with a free surface. They report that the cross-stream vortices are formed when the vortex sheet that rolls up to produce the vortex pair is perturbed by placing a rapid deceleration in the otherwise smooth motion of the flaps. Locke *et al.* find an average spacing, $\bar{L}/\delta_0$, of 0.18 (± 0.08) for the cross-stream vortices which compares well to the present results. Their results also compare well with the spacing between streamwise vortices in a plane mixing layer of 0.19 (± 0.07), when non-dimensionalized with the distance between spanwise vortices (see Jimenez, Cogallos & Bernal 1985). Locke *et al.* hypothesize that a Rayleigh-type instability is responsible for the formation of the cross-streams vortices, for which there is no theory.

7. Summary and conclusions

The major results of the present investigation, which is restricted to low Froude numbers ($\approx$ 0.1–0.2) and moderate Reynolds numbers ($\approx$ 10000–20000), are as follows.

(i) A vortex pair generator consisting of a pair of counter-rotating flaps was devised that is capable of producing laminar, repeatable vortex pairs to study the two-dimensional aspects of the interaction of a pair of trailing vortices with a free surface.

(ii) Surface contamination was shown to have a significant effect on the vortex pair or trailing vortices interacting with the free surface. Surface contamination generates opposite-signed vorticity at the free surface which can roll up into secondary vortices with approximately $\frac{1}{3}$ of the circulation of the primary vortices. The opposite-signed vorticity caused the vortex pairs to rebound from the free surface. When the surface was highly contaminated, the trajectory of the primary vortices was similar to the trajectory measured beneath a solid (no slip) surface. In the present experiments a pair of Reynolds ridges were always formed on the free surface except for highly contaminated surfaces.

(iii) Free-surface deformations, striations (see Sarpkaya & Henderson 1985), were shown to be caused by cross-stream vortices near the surface elongated in the strain

field above and between the primary vortices. The striations were often observed to form pairs which result from the interaction with their images. The spacing between the striations, of the order of $\bar{L}/\delta_0 = 0.18$, produced during the interaction of trailing vortices with the free surface was found to decrease as the Reynolds number increased and show good agreement with those from Locke *et al.* (1993) but not the spacing, $0.38 < \bar{L}/\delta_0 < 0.63$, reported by Sarpkaya & Suthon (1991).

(iv) Free-surface depressions, scars, were observed above each primary vortex and when the surface was contaminated; scars were also observed above the secondary vortices and were stronger than those above the primary vortices.

We would like to acknowledge one of the reviewers for helpful comments on the origin of the striations. Constructive interaction with Professors G. Tryggvason, L. P. Bernal and other members of the PSH has been of great assistance in the conception of the experiments, analysis of the PIV images and interpretation of the experimental findings. This work was supported by the Program in Ship Hydrodynamics (PSH) at the University of Michigan, funded by the University Research Initiative of the Office of Naval Research (contract No. N000184-86-K-0684).

REFERENCES

BARKER, S. J. & CROW, S. C. 1977 The motion of two-dimensional vortex pairs in a ground effect. *J. Fluid Mech.* **82**, 659–671.

BERNAL, L. P., HIRSA, A., KWON, J. T. & WILLMARTH, W. W. 1989 On the interaction of vortex rings and pairs with a free surface for varying amounts of surface active agent. *Phys. Fluids* A **1**, 2001–2004.

DU NOÜY, P. L. 1991 A new apparatus for measuring surface tension. *J. Gen Physiol.* **1**, 521–524.

DURAND, W. F. 1943 *Aerodynamic Theory*, vol. II. Dover.

GAINES, L. G. 1966 *Insoluble monolayers at liquid–gas interfaces.* Interscience.

HARVEY, J. K. & PERRY, F. J. 1971 Flow field produced by trailing vortices in the vicinity of the ground. *AIAA J.* **9**, 1659–1660.

HIRSA, A. 1990 An experimental investigation of vortex pair interaction with a clean or contaminated free surface. PhD thesis, Dept of Aerospace Engng, University of Michigan.

HUNT, J. C. R. 1984 Turbulent structure and turbulent diffusion near gas–liquid interfaces. In *Gas Transfer at Water Surfaces* (ed. W. Brutsaert & G. H. Jirka), pp. 67–82. D. Reidel.

JIMENEZ, J., COGOLLOS, M. & BERNAL, L. P. 1985 A perspective view of the plane mixing layer. *J. Fluid Mech.* **152**, 125–143.

KOMORI, S., UEDA, H., OGINO, F. & MIZUSHINA, T. 1982 Turbulence structure and transport mechanism at the surface in an open channel flow. *Intl J. Heat Mass Transfer* **25**, 513–521.

KWON, J. T. 1989 Experimental study of vortex ring interaction with a free surface. PhD thesis, Dept of Aerospace Engng. University of Michigan.

LAMB, H. 1932 *Hydrodynamics*, 6th edn. Cambridge University Press.

LOCKE, C. A. 1993 Origin and evolution of cross-axis vorticity in perturbed vortex pairs. MS thesis, Dept Mech. Engng, Aero. Engng & Mech., Rensselaer Polytechnic Inst.

LOCKE, C. A., HIRSA, A. & RUBIN, M. D. 1993 Short-wave instability in a laminar vortex pair. In *ASME Fluids Engng Conf., Forum on Unsteady Flows* (ed. W. L. Keith & T. Wei), FED-Vol. 157, pp. 73–81.

MUNK, W. H., SCULLY-POWER, P. & ZACHARIASEN, F. 1987 Ship wakes from space. *Proc. R. Soc. Lond.* A **412**, 231–254.

OHRING, S. & LUGT, H. J. 1991 Interaction of a viscous vortex pair with a free surface. *J. Fluid Mech.* **227**, 47–70.

SAFFMAN, P. G. 1979 The approach of a vortex pair to a plane surface in inviscid fluid. *J. Fluid Mech.* **92**, 497–503.

SARPKAYA, T. & HENDERSON, D. O. 1985 Free surface scars and striations due to trailing vortices generated by a submerged lifting surface. *AIAA Paper* 85-0445, *AIAA 23rd Aerospace Sci. Mtg. Jan. 1985 Reno, Nevada.*

SARPKAYA, T. & SUTHON, P. 1991 The interaction of a vortex couple with a free surface. *Exps Fluids.* **11**, 205–217.

SCOTT, J. C. 1975 The preparation of water for surface clean fluid mechanics. *J. Fluid Mech.* **69**, 339–351.

SCOTT, J. C. 1982 Flow beneath a stagnant film on water: the Reynolds ridge. *J. Fluid Mech.* **116**, 283–296.

TRYGGVASON, G. ABDOLLAHI-ALIBEIK, J., WILLMARTH, W. W. & HIRSA, A. 1992 Collision of a vortex pair with a contaminated free surface. *Phys. Fluids* A **4**, 1215–1222.

TRYGGVASON, G., UNVERDI, S. O., SONG, M. & ABDOLLAHI-ALIBEIK, J. 1991 Interaction of vortices with a free surface and density interfaces. In *Vortex Dynamics and Vortex Methods* (ed. C. R. Anderson & C. Greengard), pp. 679–699. Lectures in Applied Mathematics, vol. 28. AMS.

YAMADA, H. & HONDA, Y. 1989 Wall vortex induced by and moving with a confined vortex pair. *Phys. Fluids* A **1**, 1280–1282.

YU, D. & TRYGGVASON, G. 1990 The free-surface signature of unsteady, two-dimensional vortex flows. *J. Fluid Mech.* **218**, 547–572.